Advances in Science and Technology Research Journal

Advances in Science and Technology Research Journal, 2026, 20(4), 22–34
https://doi.org/10.12913/22998624/213627
ISSN 2299-8624, License CC-BY 4.0

Received: 2025.09.02
Accepted: 2026.02.15
Published: 2026.03.01

Analysis of mechanical properties and damage of polymer fibre-reinforced concrete under post-fire conditions based on acoustic emission technology

Anna Adamczak-Bugno[1], Sebastian Lipiec[2*], Jakub Adamczak[1]

[1] Faculty of Civil Engineering and Architecture, Kielce University of Technology, Al. 1000-lecia Państwa Polskiego 7, 25-314 Kielce, Poland
[2] Faculty of Mechatronics and Mechanical Engineering, Kielce University of Technology, Al. 1000-lecia Państwa Polskiego 7, 25-314 Kielce, Poland
* Corresponding author's e-mail: slipiec@tu.kielce.pl

Keywords: acoustic emission, reinforced concrete, post-fire conditions, three-point bending tests.

ABSTRACT

This article discussed the post-fire damage to concrete materials by analysing the mechanical parameters and damage mechanisms of concrete reinforced with polypropylene (PP) fibres. The tested material is offered as a construction product and is approved for sale. The effect of different fire temperatures on the material performance was analysed in laboratory tests using the acoustic emission (AE) method. The analyses showed that the samples stored under ambient conditions exhibited ductile flexural fracture, whereas those exposed to fire temperatures exhibited brittle fracture. The number of AE cracks is strongly correlated with loading conditions. The b value effectively indicates the nature of the damage, serving as an early warning indicator. AF-RA images suggest that fire temperatures accelerate and intensify shear cracking. The AE method has potential as a diagnostic technology for post-fire conditions in PP fibre-reinforced concrete.

INTRODUCTION

Concrete is widely used in construction, but its properties degrade under extreme conditions, such as fire and high temperatures. The factors influencing the degree of concrete damage at high temperatures include, among others, the rate of temperature rise, maximum temperature, exposure time, cooling rate, post-cooling conditions, and structural loading. In practice, these conditions can be difficult to predict and control, complicating the assessment of the resistance of concrete to heat [1–4].

High temperatures negatively impact the properties of most cement composites. Concrete structures may also be susceptible to thermal spalling, also known as spalling. This phenomenon affects the concretes with a low water-to-cement ratio, high compressive strength, and a dense cement matrix. It leads to the detachment of large fragments, reducing the load-bearing capacity of the structure and posing a safety risk to rescuers [5,6].

Effective methods of protection against thermal spalling include the use of thermal barriers (e.g., fireproof insulation), the addition of polypropylene (PP) fibres, air-entraining agents, and low-thermal-expansion aggregates. Numerous studies confirm the positive effect of PP fibres on spalling reduction [7,8].

The addition of PP fibres in the amount of 1–2 kg/m³ (which is approximately 0.4–0.8% of the cement paste volume) allows the formation of channels after the fibres melt, through which water vapour is released, which prevents pressure build-up and the explosion of spatter. Optimal fibre dispersion in the mixture is ensured by the coatings that reduce the hydrophobicity of the

fibres (e.g., fatty acid esters) [9,10]. Concrete damage during a fire depends on factors such as structural and material parameters as well as the temperature curve. Assessing the technical condition after a fire requires an analysis of the reduced load-bearing capacity of the structure, based on reduced material parameters. This allows for decisions to be made about repairing or strengthening the structure, rather than demolishing it [11–13].

Diagnosing the condition of concrete after fire involves in-situ and laboratory testing. Non-destructive methods, such as ground-penetrating radar (GPR) and magnetic surface wave analysis (MASW), enable the assessment of material properties and the localisation of damage. However, these technologies require further research in the context of fire. Laboratory tests to determine the depth of degradation and mechanical properties of concrete include microscopy, X-ray diffraction, thermoluminescence, and chemical analysis [14,15].

Acoustic emission (AE) is an increasingly common method for monitoring the condition of concrete structures. AE detects micro-movements and the development of defects, enabling assessment of the entire element and localisation of damage. Due to its high sensitivity, this method is useful in identifying destructive processes under load, including in the concretes modified with PP fibres. Research results also indicate that AE can be an effective tool for assessing the technical condition of concrete after a fire, opening up new directions in the diagnostics of building materials and structures [16–20].

The procedures for the use of AE are codified in technical standards [21,22]. AE studies are conducted for in-situ monitoring of concrete structures and laboratory evaluation of building materials. AE allows the detection of elastic waves generated by sudden local changes in the material resulting from deformation, crack initiation, and microstructural transformations. This method provides precise information on the time and load of damage, enabling analysis of the entire material volume [23–28].

The AE methodology enables accurate characterisation of material damage by analysing waveform features. According to the literature, the mechanisms and extent of concrete damage can be assessed using AE parameters, such as ringing counts, energy, b-value analysis, and AF-RA correlation analysis [29–31]. Previous studies on PP fibre-reinforced concrete using the acoustic emission method have primarily focused on determining the effect of varying the content of reinforcing fibres, additives, and admixtures on the acoustic activity of materials. The effect of fire temperatures on PP-reinforced concrete has also been analysed. Changes in the acoustic response of samples have been examined, with a focus on the analysis related to the division of recorded signals into classes and the assignment of individual groups of events to processes occurring in the material structure [17,32–34].

In addition to the AE-based analyses, several studies have examined the thermal performance, failure mechanisms, and rehabilitation of structural members exposed to high temperatures. Abdullah and Lateef [35] presented an innovative method for reinforcing beams made of different types of concrete using cross-rod steel bracing under pure torsion, highlighting improved load transfer and ductility. Major et al. [36] investigated the heating of steel structures during fire loading, providing important insights into thermal gradients and heat transfer mechanisms relevant to composite concrete–steel behaviour. Djamaluddin et al. [37] analysed the flexural behaviour of repaired reinforced concrete beams damaged by reinforcement corrosion and strengthened using grouting and FRP sheet systems, which may also serve as effective techniques for post-fire rehabilitation. These studies broaden the background of post-fire structural performance and complement AE-based approaches aimed at damage diagnosis and strength evaluation.

This article discussed three-point bending tests performed on PP fibre-reinforced concrete stored at ambient temperature and exposed to fire temperatures. The acoustic emission method was used in the study. The mechanical strength and deformation under load of the material were analysed, along with the failure mechanism. The influence of the specified conditions on commonly used indicators in the acoustic emission method was also verified. This approach demonstrated differences and provided a preliminary assessment of the feasibility of using the acoustic emission method in assessing PP concrete in post-fire conditions. No similar research approach has been undertaken to date.

MATERIALS AND METHODS

Materials

The tests were conducted on concrete beams measuring 50 × 50 × 300 mm. The material was

composed of concrete with the addition of dispersed polypropylene fibres. The general parameters of the mix are as follows: cement CEM I 42.5 R (≈349 kg/m³), water-to-cement ratio 0.49, aggregate fractions 0/4–48%, 4/8–9.5%, 8/16–42.5%, PCE-type superplasticiser ≈0.32% by cement weight, air content ≈1.25%, and density ≈2406 kg/m³. Polypropylene fibres (12–19 mm, 0.6–0.9 kg/m³) were added according to EN 14889-2 recommendations.

Four series of samples were tested. The samples from the first group (PPR) were stored at ambient room temperature (±20 °C). The samples from the second test series (PPF1) were fired in a laboratory furnace. The processing temperature was 300 °C. The holding time from reaching the target temperature was 3 hours. The samples from the third test series (PPF2) were fired in a laboratory furnace at 450 °C. The holding time from reaching the target temperature was 3 hours. The samples from the fourth test series (PPF3) were fired in a laboratory furnace at 600 °C. Once the target temperature was reached, the samples were held for 3 hours to achieve a nearly uniform core temperature before cooling and testing. This approach is consistent with steady-state testing, where the temperature is "held until a thermal steady state is reached," and falls within the typical soak times reported in the literature (1–3 hours depending on the test program) [38,39].

Methods

Mechanical performance test

According to ASTM procedure [21] three-point bending tests were performed sequentially. A Zwick-Roell servo-driven electric testing machine was used, with a loading speed of 0.5 mm/min. During the real-time tests, the following signals were recorded: test time, load force on the sample, and displacement of the strength testing machine traverse. As a result of the three-point bending test, the stress-strain relationships in the nominal system were determined.

AE monitoring method

The AE monitoring system is shown in Figure 1. The system consisted of an AEWin Express-8 processor and two Vallen VS75-SIC-34 dB sensors. Each sensor had a built-in preamplifier. Technical silicone was used as the coupling medium. To exclude excessive external interference [17,19], a 45 dB threshold was used. Data collection occurred at a frequency of 1 MHz. The data were displayed in real time on a computer screen and saved immediately after testing.

Analysis of acoustic emission (AE) parameters

AE signals collected by the system are characterised by energy and frequency parameters. For the analyses presented in this manuscript, the number of impacts (RC), amplitude (A), rise time (RT), and duration (D) were taken into account directly and indirectly (Figure 1). RC refers to the acoustic activity level (AE), correlating with the intensity of internal concrete damage development and its real-time changes. A is related to the maximum instantaneous value of the AE signal and reflects the intensity of individual AE events related to crack propagation and transformation. RT and D capture the dynamic material damage process and enable inference regarding the crack damage pattern [29,31]. The choice of these parameters stems from the well-established use of these indicators in concrete testing. This approach is supported by the literature [30,40,41].

The initiation and development of internal defects and cracks in the cement matrix is associated with the formation of AE events (as elastic waves) with variable amplitude. Therefore, the relative *b-value* can be used to assess the degree of damage to the concrete [29]. Equation 1 presents a method for calculating the *b-value* according to the Gutenberg-Richter law [29]. Considering that the *b-value* is sensitive to fine cracks, which affects the speed of analysis, the *b-value* calculation was performed using a group of 50 AE impacts.

Concrete failure in bending results from the combined effect of tension and shear. By analysing the rise angle (RA) and mean frequency (AF), the main failure mode of the structure can be identified. The formulas for calculating both parameters are presented in Equations 2 and 3 [29–31]. In tensile failure, elastic energy is released rapidly, resulting in short RT and D times and high A. This results in the relationship RA < AF. In shear failure, energy is dissipated through sliding friction of cracks, which is associated with longer RT and D times and leads to the relationship RA > AF. The diagonal of the graph can be used as a mode boundary (Figure 1) [31].

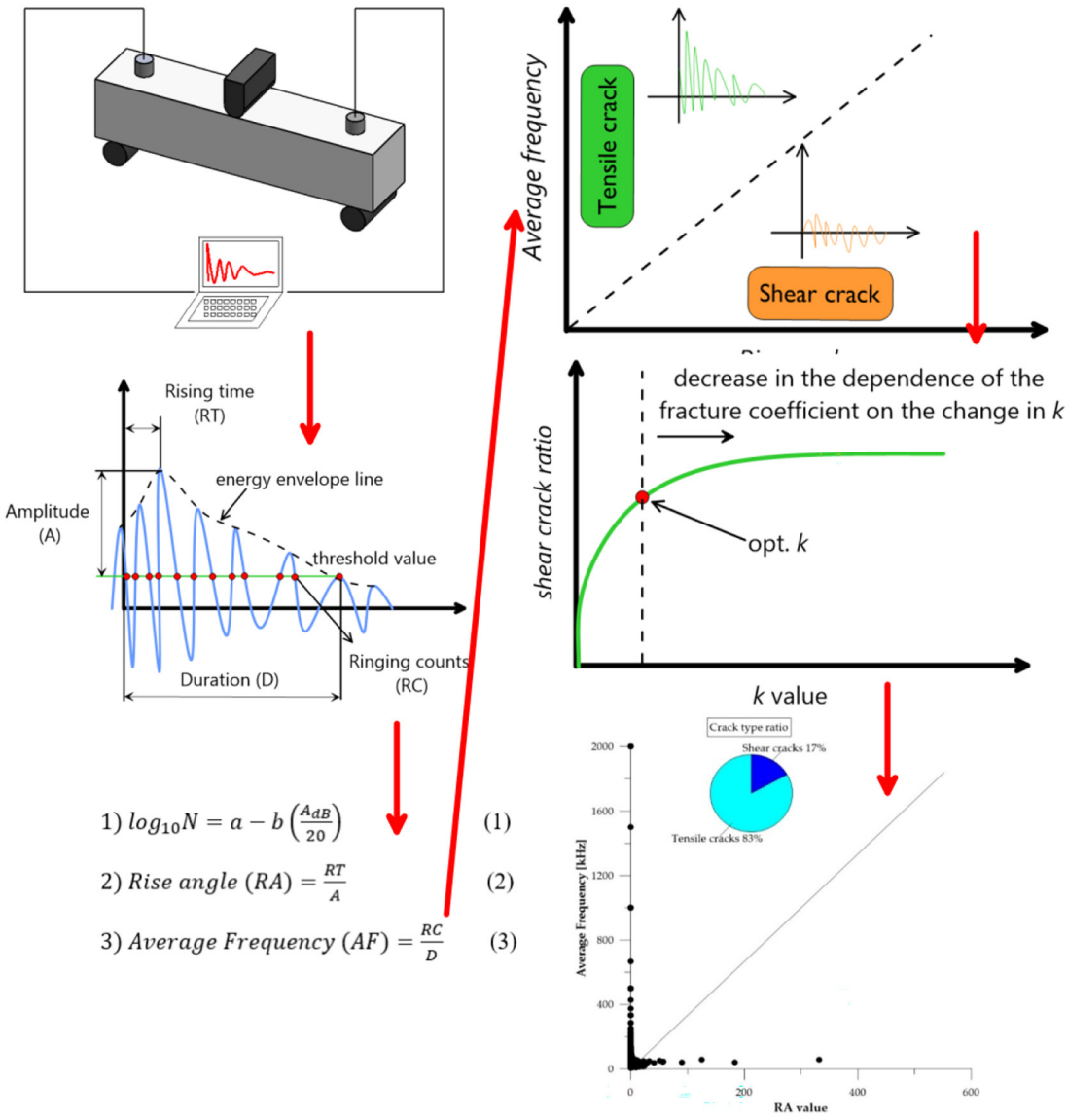

Figure 1. Schematic diagram of the research

RESULTS AND DISCUSSION

Stress-strain relationships

In order to determine the behaviour of the analysed material under load, a laboratory testing programme was developed. It included tests carried out according to a three-point bending test scheme. Samples in the form of beams with nominal dimensions of L = 300 mm, B = 50 mm, W = 50 mm (according to the diagram in Figure 2 were prepared for testing [42]. The samples were made of polypropylene (PP) fibre-reinforced concrete, which was exposed to fire temperatures according to the assumptions presented in the first part of this work. The laboratory tests were accompanied by the recording of acoustic emission signals. As a result of three-point bending tests carried out on the samples made of polypropylene fibre-reinforced concrete (PP), nominal stress-strain relationships were determined using the following relationships:

$$M_b = \frac{FS}{4} \tag{4}$$

$$\sigma_{nom} = \frac{6M_b}{BW^2} \tag{5}$$

$$\varepsilon_{nom} = \frac{6uB}{S^2} \tag{6}$$

where: M_b – bending moment; F – load applied to the sample (beam); S – spacing between supports in the test; σ_{nom} – nominal stress; B – sample thickness; W – sample height; ε_{nom} – nominal strain; u – sample deflection.

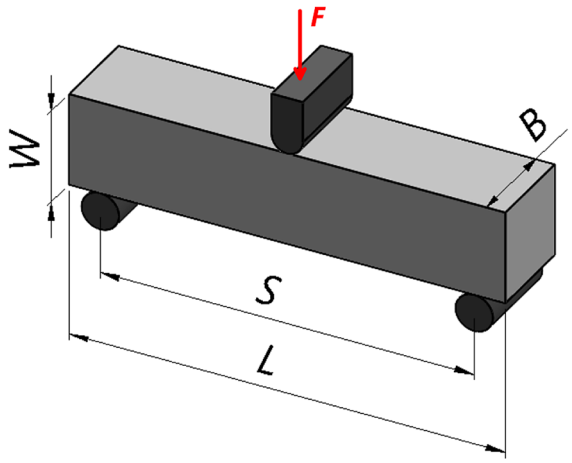

Figure 2. Schematic diagram of samples accepted for three-point bending tests

The nominal curves in the stress-strain relationship determined as a result of three-point bending tests are shown in Figure 3a. The highest level of nominal stresses was characteristic of the PP fibre-reinforced concrete in its initial state (without temperature influence), amounting to 15 MPa. Exposing the concrete material to a fire temperature of 300 °C (PPF1) resulted in a reduction in stresses of approx. 28% in the three-point bending test, to a level of approx. 11 MPa. On the other hand, the nominal deformations at the moment of failure increased twice for the annealed material compared to the initial material. A significant decrease in stresses occurred when the annealing temperature of concrete was increased above 300 °C (i.e. 450 °C and 600 °C). In both cases (PPF2 and PPF3), the nominal stresses did not exceed 0.4 MPa. Exposing the PP fibre-modified concrete to increasingly higher temperatures led to a significant increase in the deformation values at the moment of sample failure during the test. This is identified with the impact on the ductility of the finished material of the PP fibres used, which undergo increasing melting as a result of thermal exposure.

Important partial information from the point of view of the adopted methodology for assessing the impact of fire temperatures on the PP fibre-modified concrete can be obtained by analysing the condition of the samples after three-point bending tests (Figure 3b, c, d, e). When testing the initial material (PPR) and the samples exposed to heat at a temperature of 300 °C, no

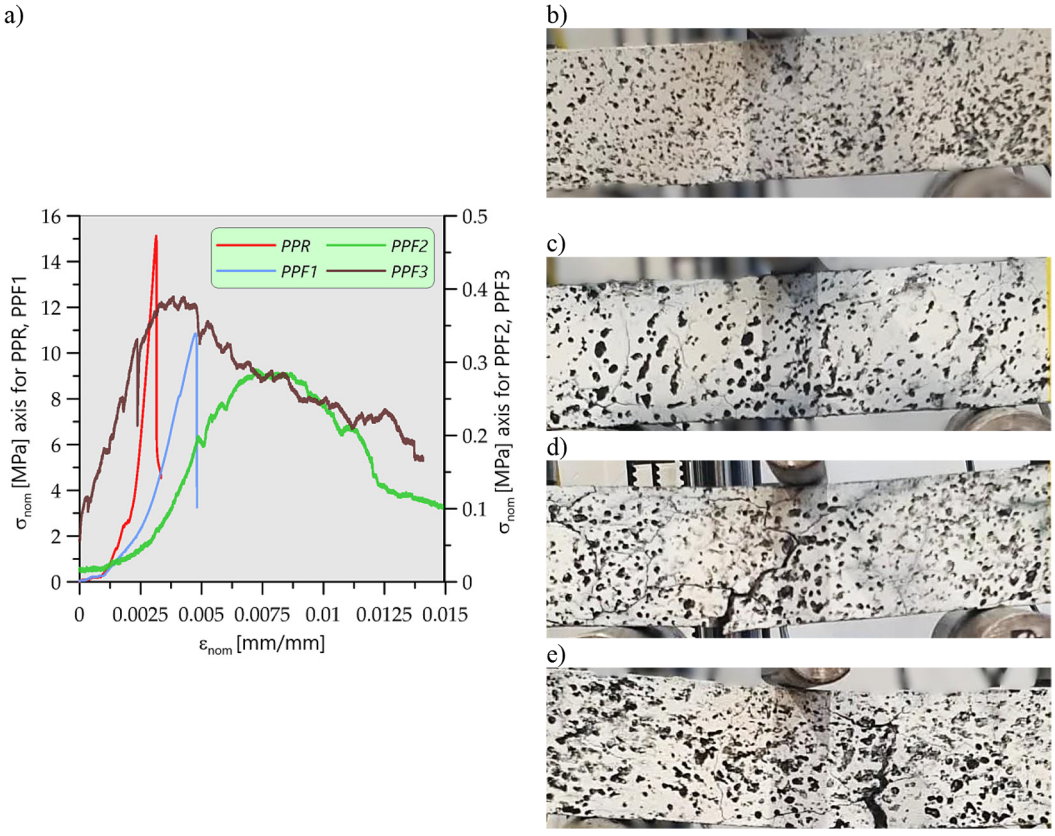

Figure 3. Results of three-point bending tests: (a) stress-strain relationship, views of the samples after testing for material marked: (b) PPR, (c) PPF1, (d) PPF2, (e) PPF3

significant cracks or spalling of the material were observed (Figure 3b, c). The macroscopic appearance of the samples after testing differed for the PPF2 and PPF3 heat exposure variants. In both cases, cracks spreading across the surface of the samples are visible, changing direction as the load progresses. For the samples annealed at 450 and 600 °C, the cracks were located at the lower edges of the samples (Figure 3 d, e). The results of the laboratory tests have become a valuable source of information which, together with acoustic emission signal analyses, will allow for the assessment of PP fibre-modified concrete after exposure to fire temperatures.

Damage characterisation based on AE signals

Ringing counts

Figure 4 presents the evolution of ringing counts and load over time for all samples subjected to bending. The table summarises the characteristic points of the failure process – the end of the elastic range, the moment of maximum load, and the point of fracture. A combined analysis of these parameters makes it possible to assess the relationship between load development and the acoustic activity of the material.

For the PPR (reference) sample, the end of the elastic range occurs at approximately 2358 s, at a load of about 2484 N. At this point, a noticeable increase in ringing counts is observed, corresponding to the initiation of microcracks in the cement matrix. Subsequently, the number of counts increases progressively along with the rising load, up to the point of maximum load. At the peak load, a rapid increase in AE activity occurs, caused by fibre debonding and pull-out processes, as polypropylene fibres start to transfer stresses across the cracks [18,20]. After exceeding the maximum load, both the load and AE activity decrease. At the fracture point (around 3456 s), a short and intense AE burst corresponds to the final rupture of the specimen.

In the case of PPF1 (heated to 300 °C), the end of the elastic range appears much earlier – after about 585 s – and the maximum load reaches 642 N, with complete failure at 651 s. Despite the lower load capacity, the AE pattern is similar

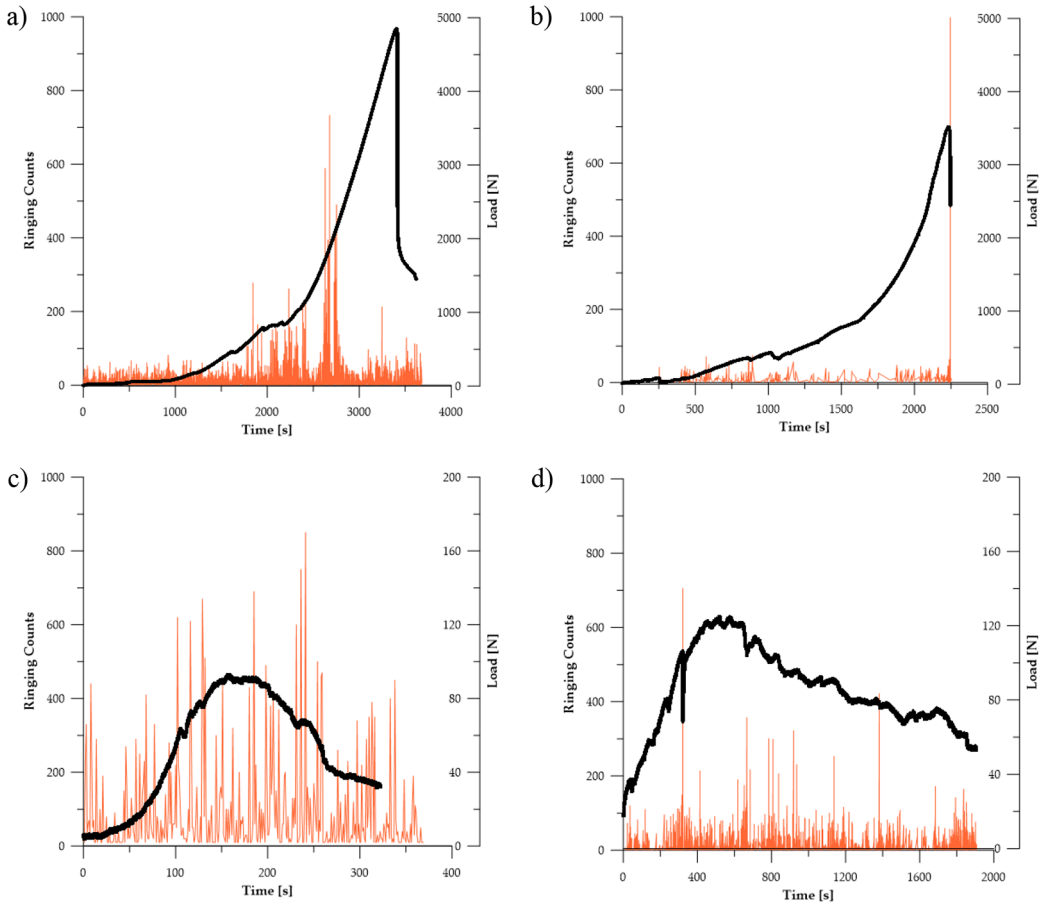

Figure 4. Bending load-time curves with ringing counts results: (a) PPR, (b) PPF1, (c) PPF2, (d) PPF3

to that of the reference sample: a distinct increase in ringing counts during the transition from elastic to plastic behaviour and a sharp rise near the maximum load. This suggests that PP fibres did not undergo significant oxidation at 300 °C and retained their ability to bridge cracks and transfer stresses [18,20].

For the PPF2 sample (450 °C), the end of the elastic range occurs at 825 s, with a corresponding load of about 997 N. Elevated AE activity is already observed at this stage, indicating early microcracking and partial degradation of the fibre–matrix interface. At maximum load, AE activity remains high but irregular, suggesting dispersed matrix cracking and weakened bonding between the fibres and the cement matrix. After reaching the load peak, the load decreases gradually, while the AE activity remains moderate — the absence of a pronounced AE burst at fracture (around 2007 s) confirms a progressive, non-brittle failure mechanism. The PPF3 sample (600 °C) exhibits the most distinct behaviour. The end of the elastic range occurs very early (361 s) at a maximum load of only 585 N. At this stage, AE activity is already elevated and scattered, indicating premature cracking of the degraded matrix and a complete loss of fibre–matrix adhesion. No significant increase in AE activity is observed at the maximum load – the AE signals remain moderate, confirming that the fibres no longer effectively transfer stresses. During fracture (around 1900 s), AE activity remains low and steady, corresponding to a slow and diffused degradation process typical of materials without active fibre reinforcement. In summary, as the exposure temperature increases, a clear decrease in maximum load (from ~2484 N for PPR to ~585 N for PPF3) and a shortening of the elastic phase are observed. Simultaneously, the character of AE activity changes – from distinct, event-driven emissions in PPR and PPF1 to diffuse, irregular AE activity in PPF2 and PPF3. The relationship between load and ringing counts at characteristic points clearly confirms the degradation of PP fibres and the loss of their ability to effectively bridge cracks under high-temperature conditions, consistent with the mechanisms described in previous studies [18,20].

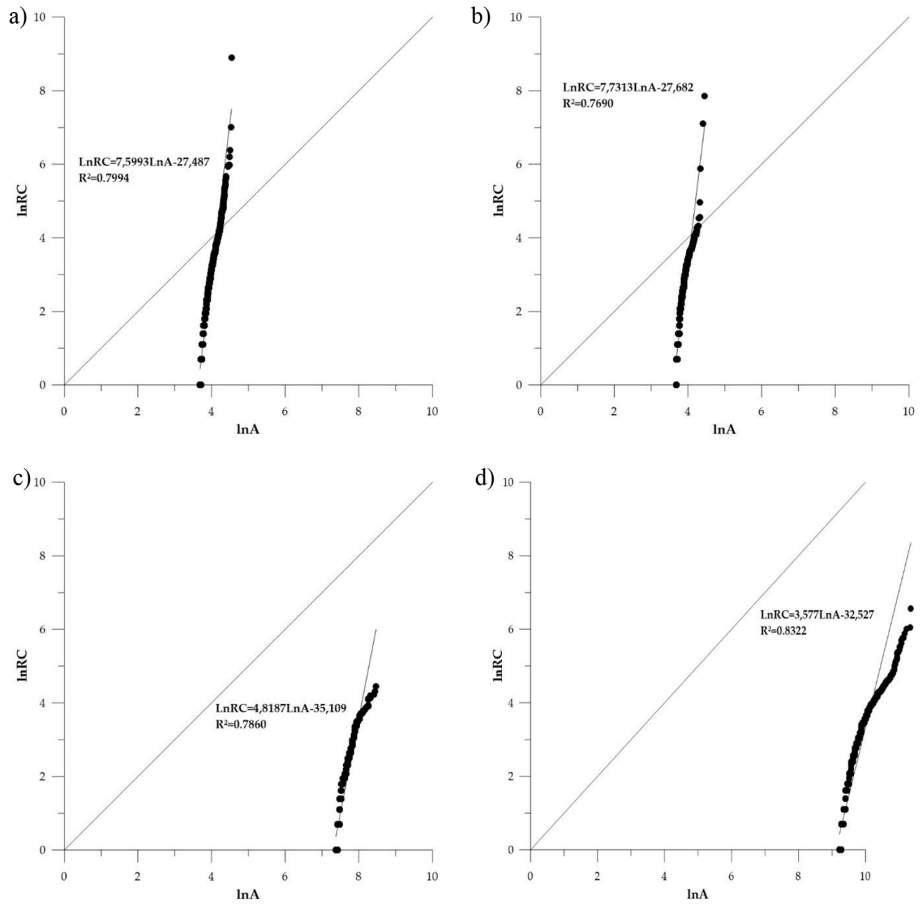

Figure 5. Dependence of lnA and lnRC for PPR and PPF samples: (a) PPR, (b) PPF1, (c) PPF2, (d) PPF3

Amplitude versus ringing counts

The number of ringing events directly relates to the frequency of events in the damage process. In turn, the amplitude is related to the intensity of individual AE events. Analysing the correlation between amplitude and the number of ringing events allows us to draw conclusions about the development of concrete damage under load.

Figure 5 shows the lnA-lnRC relationship for the PPR and PPF samples under bending. The linear fit coefficient R^2 measures the correlation between these two parameters. When analysing the obtained results, it can be concluded that the correlation of these characteristics for the sample stored at ambient temperature and the fired samples is similar. The strong correlation between lnA and lnRC under bending load refers to the homogeneous internal structure of the material.

The slope of the linear fit for the PPR and PPF1 samples is higher than for the PPF2 and PPF3 samples. The smaller exponent for the samples exposed to 450 °C and 600 °C indicates that the number of acoustic emission events increased with amplitude, but at a slower rate than for the sample stored at room temperature and fired at 300 °C.

It can be assumed that the fibres fired at temperatures of 450 °C and 600 °C led to the formation and development of microcracks in the cement matrix and the propagation of macrocracks. This resulted in the recording of acoustic emission signals similar to those observed in "pure" concrete without fibres. The damage process was more "single-stage" and less complex than in concrete with fibres, as there was no mechanism for fibres to "bridge" cracks.

The smaller exponent for samples PPF2 and PPF3 indicates that in the concrete where fibres oxidized due to fire temperatures, major damage appears relatively faster, and acoustic emission during the crack development phase is less complex. It was found that in the material exposed to 450 °C and 600 °C, the cracking and damage development process was more "step-like" and had fewer stages – cracks formed and developed rapidly, resulting in fewer but stronger emission signals. The fibres in samples PPR and PPF1 acted as stress bridges – slowing macrocrack development and causing more microscopic damage. The absence of this mechanism in the concrete with oxidised fibres means that cracks propagate faster, but there are fewer "microscopic" emission events.'

B-value analysis

Fig. 6 presents the variation of the b-value for the PPR and PPF samples subjected to bending loads. The b-value characterizes the nature and scale of damage in the material – high b-values indicate the dominance of microcracking, while low b-values correspond to the formation and propagation of macrocracks [29].

For the PPR (reference) sample, the b-value initially reached approximately 1.6–1.8, corresponding to low-energy AE events associated with microcracking of the cement matrix and the onset of fibre debonding. As the load increased (up to about 5000 N), the b-value gradually decreased to around 0.8–1.0, indicating damage concentration and the growth of larger cracks. In the final stage, just before failure (around 3450 s), the b-value exhibited local fluctuations, reflecting the unstable propagation of the dominant crack. This behaviour confirms that the material transitioned from dispersed microcracking to failure governed by a major macrocrack.

In the PPF1 sample (heated to 300 °C), the evolution of the b-value was similar to that of the reference sample. Initially, the b-value reached around 1.6, corresponding to low-energy AE events caused by friction and partial pull-out of fibres from the matrix. As the load increased (up to about 3200–3400 N), the b-value showed a gradual decrease but remained above 1.0, indicating a dispersed damage pattern. Near the maximum load, a sudden drop followed by short fluctuations in b-value occurred, corresponding to the initiation and development of the main crack. This confirms that PP fibres were not significantly degraded at 300°C and continued to bridge cracks effectively, resulting in a more ductile and controlled failure mechanism.

For the PPF2 sample (450 °C), the b-value started at around 1.2, suggesting the predominance of microcracking in the weakened and partially degraded matrix. As the load increased (up to about 1000 N), the b-value rapidly dropped to 0.6–0.8, indicating damage concentration and the formation of larger cracks. After reaching the maximum load, the b-value remained low, demonstrating that the damage was dominated by a single macrocrack. The material lost its ability to dissipate energy, and the failure process became abrupt and localised – typical of brittle materials.

The PPF3 sample (600 °C) showed the lowest and most unstable b-values among all tested specimens. Initially, the b-value reached 1.0–1.2,

but it quickly decreased to 0.4–0.6, remaining at this low level for most of the test duration. This confirms the dominance of macrocracking from the early stages of loading. With the degradation of PP fibres and the loss of fibre–matrix adhesion, the material exhibited a fully brittle behaviour, with rapid crack propagation and limited ability to absorb or dissipate energy. The absence of a b-value increase in the final stage further confirms the complete loss of stress redistribution capability.

In summary, as the exposure temperature increased:

- the initial b-value decreased (from ~1.6–1.8 for PPR to ~1.0 for PPF3),
- the b-value dropped more rapidly with increasing load, and
- low b-values persisted until failure, indicating the dominance of macrocracks and brittle behaviour.

The evolution of the b-value over time clearly demonstrates that thermal exposure leads to PP fibre degradation and weakening of the fibre–matrix interface, which reduces the ability of a material to dissipate energy and control crack propagation. In PPR and PPF1 samples, with fibres retaining their integrity, damage was more distributed and gradual, whereas in PPF2 and PPF3 samples, failure occurred in a sudden and localised manner.

Crack evolution analysis based on AF-RA images

Figure 7 shows the AF-RA relationships and the related bending crack classification results. The results indicate that the bending failure of the PPR and PPF1 specimens occurred mainly under the conditions with a predominance of tensile cracks, whereas the failure of the material exposed to temperatures of 450 °C and 600 °C was characterised by a significantly greater proportion of shear cracks. The results also show that the density of scatter points in the low-frequency region is higher for the PPF2 and PPF3 specimens. Therefore, it can be concluded that in the

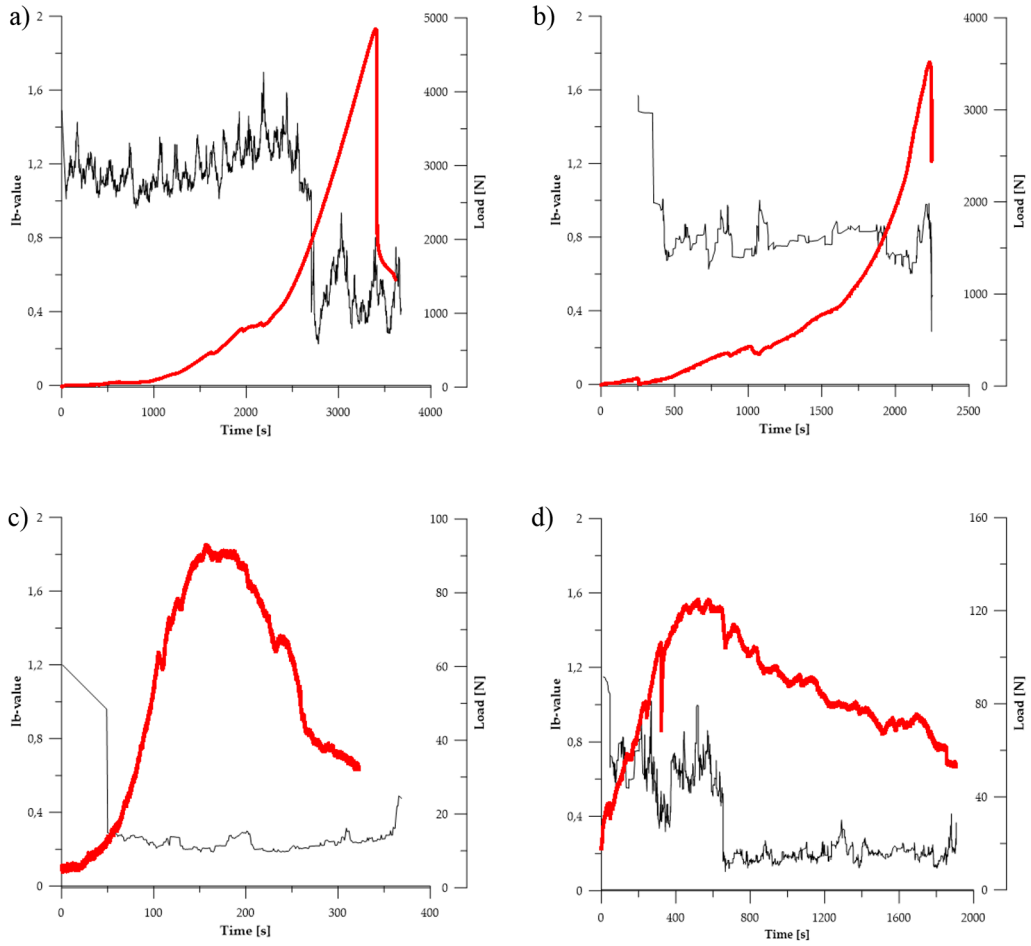

Figure 6. *B-value* acquisition results for PPR and PPF samples: (a) PPR, (b) PPF1, (c) PPF2, (d) PPF3 (Ib-value – black line; Load – red line)

specimens exposed to temperatures of 450 °C and 600 °C, in contrast to the PPR and PPF1 materials, damage occurred throughout the entire volume of the element, not only in the tensile zone.

The shear cracking rate of PPF2 and PPF3 specimens under bending loads is significantly higher than that of the PPR and PPF1 specimens. It was found that shear stress can change the crack propagation direction [29–31]. It can be observed from Figure 7 that the crack propagation paths in the specimens subjected to 450 °C and 600 °C form a larger angle with the loading direction, indicating that a larger shear stress is generated during loading, which naturally results in a larger number of shear cracks. When analysing the precise signal distribution as a function of AF-RA, it can be concluded that in the case of PPR and PPF1 specimens, high AF and low RA occurred in the initial phase – signals characteristic of tensile cracks in the matrix. In the crack propagation phase, when the fibres began to bear load, more frequent AE signals with lower AF and higher RA were observed, typical of friction and fibre pull-out. The material failure process was prolonged and not very rapid. In the final phase, average AF and higher Ra were observed than in pure concrete at the same stage.

In the case of specimens PPF2 and PPF3, high AF and low RA signals were observed during the initial loading phase. This, similarly to the PPR and PPF1 specimens, was associated with dominant tensile microcracks in the cement matrix. As cracks developed, there was a gradual decrease in AF and an increase in RA (crack development and increased friction). At failure, short, high AF peaks of various frequencies were observed – a mixed mechanism. The lack of "bridging" resulted in a rapid increase in shear signals.

Comparison of results with the literature

To generalise the obtained results, a comparison was made with the data available in the

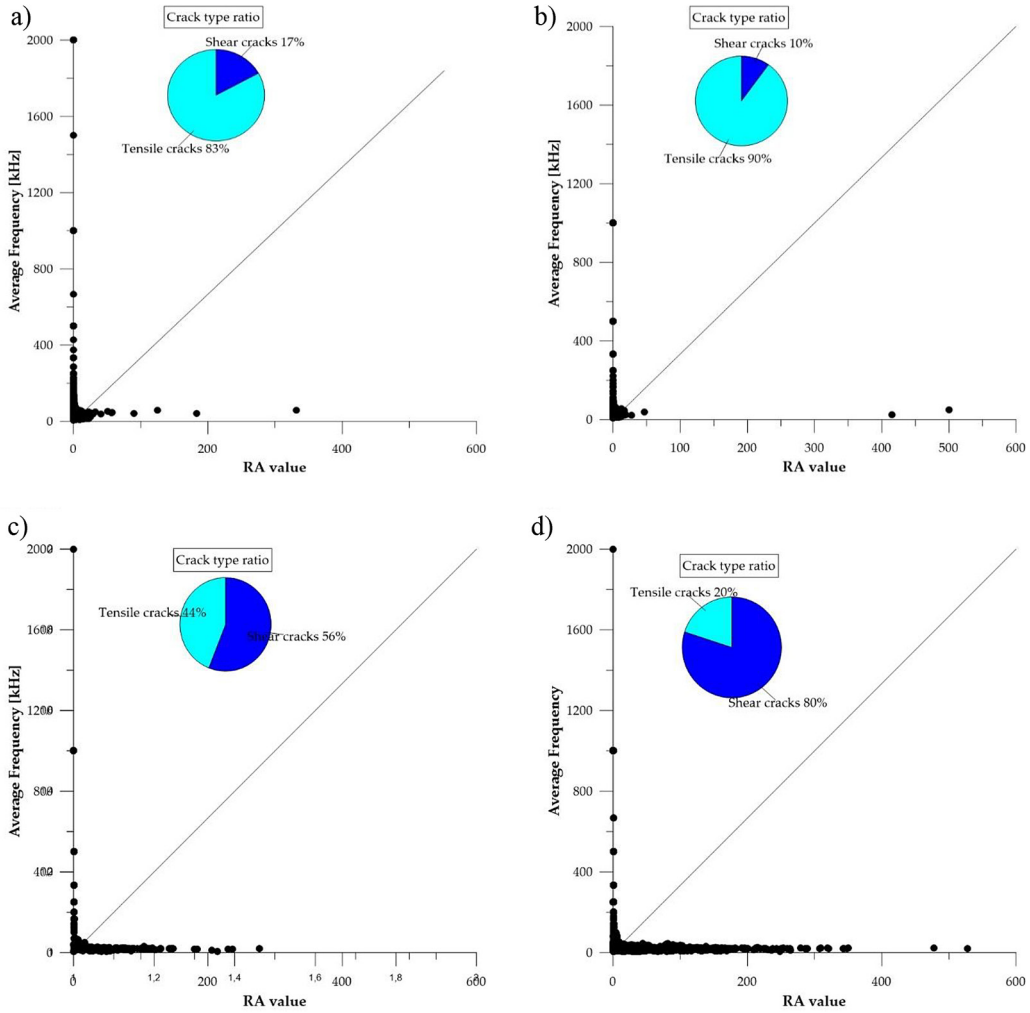

Figure 7. RF-RA relationship for PPR and PPF samples: (a) PPR, (b) PPF1, (c) PPF2, (d) PPF3

Table 1. Comparison of authors' own findings with literature [10,13,43]

Aspect	Authors' own findings (AE + three-point bending)	Kalifa et al., 2001	Hager, 2019	Resende et al., 2022
Mechanism of PP action	Gas-release channels formed after PP softening/ melting reduce spalling; effect visible up to ~300 °C.	PP addition to HPC effectively eliminates spalling; mechanism: permeability increase after PP melting.	PP mitigate spalling risk through melting (~170–180 °C) and micro-channel formation; effectiveness depends on dosage and geometry.	In HSC with PP, no spalling and improved residual performance observed.
Softening/melting temperature of PP	AE response indicates onset ~170–180 °C; above ~450 °C fibers lose function, brittle fracture dominates.	Effective below 300 °C (Tm ≈ 170–180 °C).	Review: Tm ≈ 170–180 °C; affects permeability and pore-pressure relief.	Melting - degassing - reduced degradation; effectiveness decreases at higher T.
Spalling ≤ 300 °C	No or limited spalling; AE AF–RA maps indicate tensile cracking; high b-value (microcracking).	No spalling observed in PP-HPC under standard exposures.	Confirms PP efficiency in this temperature range.	No spalling for tested mixes; consistent with present study.
> 450–600 °C	Transition to brittle behaviour; AF–RA shifts to shear/friction; b-value decreases.	PP effectiveness declines after fibre continuity loss.	Above ~450 °C, matrix damage dominates; PP cannot prevent brittleness.	Mechanical degradation increases despite earlier spalling resistance.

literature on the influence of polypropylene (PP) fibres on concrete behaviour under elevated temperatures (Table 1).

CONCLUSIONS

In summary, this article examined the effect of fire temperatures on the mechanical and acoustic properties of the PP fibre-reinforced concrete under bending loading. Three fire temperature cases (air-drying) and a reference test were analysed. The variable in the analysis was the firing temperature in a laboratory furnace. The following conclusions can be drawn from the article:

- the effect of fire temperatures on concrete material on stresses and strains in three-point bending tests has been demonstrated;
- the highest nominal stresses were obtained for the starting material (PPR). With the introduction of material annealing and an increase in temperature, the stresses decreased, with the greatest effect observed at temperatures above 300 °C;
- the strain at the moment of failure increased along with fire temperatures affecting the concrete material, which may be influenced by the degree of melting of the PP fibres;
- under the influence of bending loads, PPF2 and PPF3 show distinct strain hardening properties, which result from the PP fibre content;
- Ringing counts confirm the formation of microcracks and the presence of a fibre-matrix interface in PPR and PPF1 samples. In the case of PPF2 and PP23, ringing counts indicate a brittle failure mechanism throughout the analysed time courses;
- analysis of the lnA-lnRC relationship, *b-values* and AF-RA crack classification also indicates that the samples under post-fire bending conditions are characterised by a brittle failure mechanism with a predominance of shear cracks and rapid growth of macrocracks.

The conducted research demonstrated that some fire temperatures cause oxidation of PP fibres, reducing the mechanical strength of the material and altering its behaviour under bending loads. Using the acoustic emission method, differences were identified between the failure mechanisms of reinforced and unreinforced concrete due to thermal oxidation of fibres. The research is a prelude to future work, which will focus on research that considers the material cooling method and heating rate, and will involve larger-scale samples.

Acknowledgments

This research has been supported by the Minister of Science of Poland (projects No. 02.0.21.00/1.02.001/SUBB.BKWD.25.001 and 01.0.13.00/1.02.001/SUBB.MKKM.25.001).

REFERENCES

1. Kodur V., Properties of concrete at elevated temperatures, international scholarly research notices. 2014; e468510. https://doi.org/10.1155/2014/468510.
2. Pasztetnik M., Wróblewski R., A literature review of concrete ability to sustain strength after fire exposure based on the heat accumulation factor, Materials 2021;14:4719. https://doi.org/10.3390/ma14164719
3. Kuehnen R., Youssef M.A., El-Fitiany S.F., Influence of natural fire development on concrete compressive strength, Fire 5. 2022;34. https://doi.org/10.3390/fire5020034
4. Ma Q., Guo R., Zhao Z., Lin Z., He K., Mechanical properties of concrete at high temperature—A review, Construction and Building Materials 2015;93:371–383. https://doi.org/10.1016/j.conbuildmat.2015.05.131
5. Alaskar A., A comprehensive review on the influence of elevated temperatures on the mechanical performance of high-performance concretes, J. Umm Al-Qura Univ. Eng. Archit. 2025;16:879–890. https://doi.org/10.1007/s43995-025-00199-w
6. Mohammed H., Ahmed H., Kurda R., Alyousef R., Deifalla A.F., Heat-induced spalling of concrete: A review of the influencing factors and their importance to the phenomenon, Materials 2022;15:1693. https://doi.org/10.3390/ma15051693
7. Holan J., Novák J., Müller P., Štefan R., Experimental investigation of the compressive strength of normal-strength air-entrained concrete at high temperatures, Construction and Building Materials 2020;248:118662. https://doi.org/10.1016/j.conbuildmat.2020.118662
8. Sirisena G., Jayasinghe T., Gunawardena T., Zhang L., Mendis P., Mangalathu S., Machine learning-based framework for predicting the fire-induced spalling in concrete tunnel linings, Tunnelling and Underground Space Technology 2024;153:106000. https://doi.org/10.1016/j.tust.2024.106000
9. Resende H.F., Reis E.D., Arroyo F.N., de Moraes, M.H.M. dos Santos H.F., da Silva E.G., Lahr F.A.R., Chahud E., Panzera T.H., Christoforo A.L., Branco L.A.M.N., Residual mechanical properties and durability of high-strength concrete with polypropylene fibers in high temperatures, Materials 2022;15:4711. https://doi.org/10.3390/ma15134711
10. Kalifa P., Chéné G., Gallé C., High-temperature behaviour of HPC with polypropylene fibres: From spalling to microstructure, Cement and Concrete Research 2001;31:1487–1499. https://doi.org/10.1016/S0008-8846(01)00596-8
11. Wróblewska J., Kowalski R., Assessing concrete strength in fire-damaged structures, Construction and Building Materials 2020;254:119122. https://doi.org/10.1016/j.conbuildmat.2020.119122
12. Zahid M.M., Bakar B.A., Nazri F., Ahmad M., Muhamad K., Review of Repair Materials for Fire-Damaged Reinforced Concrete Structures, IOP Conf. Ser.: Mater. Sci. Eng. 2018;318:012023. https://doi.org/10.1088/1757-899X/318/1/012023
13. Hager I., Mróz K., Role of polypropylene fibres in concrete spalling risk mitigation in fire and test methods of fibres effectiveness evaluation, Materials 2019;12:3869. https://doi.org/10.3390/ma12233869
14. Wróblewska J., Laboratoryjne metody oceny betonu w konstrukcji po pożarze, Construction Materials 2017;1:13–15. https://doi.org/10.15199/33.2017.07.04
15. Placido F., Thermoluminescence test for fire-damaged concrete, Magazine of Concrete Research 1980;32:112–116. https://doi.org/10.1680/macr.1980.32.111.112
16. Adamczak-Bugno A., Krampikowska A., The acoustic emission method implementation proposition to confirm the presence and assessment of reinforcement quality and strength of fiber–cement composites, Materials. 2020;13:2966. https://doi.org/10.3390/ma13132966
17. Świt G., Adamczak A., Krampikowska A., Bridge management system within the strategic roads as an element of smart city, IOP Conf. Ser.: Earth Environ. Sci. 2019;214. https://doi.org/10.1088/1755-1315/214/1/012054
18. Carrasco Á., Méndez F., Leaman F., Molina Vicuña C., Short review of the use of acoustic emissions for detection and monitoring of cracks, Acoust Aust 2021;49:273–280. https://doi.org/10.1007/s40857-021-00219-4
19. Świt G., Dzioba I., Adamczak-Bugno A., Krampikowska A., Identification of the fracture process in gas pipeline steel based on the analysis of AE Signals, Materials 2022;15:2659. https://doi.org/10.3390/ma15072659
20. Kamel O.A., Abouhussien A.A., Hassan A.A.A., Abdel Aleem B.H., An evaluation of the acoustic activity emitted in fiber-reinforced concrete under flexure at low temperature, Sensors 2025;25:2703. https://doi.org/10.3390/s25092703
21. ASTM E3100-22, ASTM E3100-22, Standard Guide for Acoustic Emission Examination of Concrete Structures, ASTM International, West Conshohocken, 2022. www.astm.org
22. ISO 16837:2019, ISO 16837:2019, Non-destructive testing – Acoustic emission testing – Test method for damage qualification of reinforced concrete beams, International Organization for Standardization, Geneva, 2019.

23. Chinh L.M., Adamczak A., Krampikowska A., Świt G., Dragon bridge - the world largest dragon-shaped (ARCH) steel bridge as element of smart city, E3S Web Conf. 2016;10:00106. https://doi.org/10.1051/e3sconf/20161000106
24. Ning X., Li J., Li Y., An explorative study into the influence of different fibers on the spalling resistance and mechanical properties of self-compacting concrete after exposure to elevated temperatures, Applied Sciences 2022;12:12779. https://doi.org/10.3390/app122412779
25. Raczkiewicz W., Wojcicki A., Grzmil W., Zapala-Slaweta J., Impact of Environment Conditions on the Degradation Process of Selected Reinforced Concrete Elements, IOP Conf. Ser.: Mater. Sci. Eng. 2019;471:032048. https://doi.org/10.1088/1757-899X/471/3/032048
26. Świt G., Krampikowska A., Tworzewski P., Non-destructive testing methods for in situ crack measurements and morphology analysis with a focus on a novel approach to the use of the acoustic emission method, Materials 2023;16:7440. https://doi.org/10.3390/ma16237440
27. Tworzewski P., Goszczynska B., An application of an Optical Measuring System to Reinforced Concrete Beams Analysis, in: 2016 Prognostics and System Health Management Conference (PHM-Chengdu), 2016;1–6. https://doi.org/10.1109/PHM.2016.7819937
28. Tworzewski P., Teodorczyk M., Tworzewska J., Tracking of Crack Formation in Concrete Using Acoustic Emission Method and Digital Image Correlation, IOP Conf. Ser.: Mater. Sci. Eng. 2019;471:052032. https://doi.org/10.1088/1757-899X/471/5/052032
29. Colombo I.S., Main I.G., Forde M.C., Assessing damage of reinforced concrete beam using "b -value" analysis of acoustic emission signals, Journal of Materials in Civil Engineering 2003;15:280–286. https://doi.org/10.1061/(ASCE)0899-1561(2003)15:3(280)
30. Aggelis D.G., Classification of cracking mode in concrete by acoustic emission parameters, Mechanics Research Communications 2011;38:153–157. https://doi.org/10.1016/j.mechrescom.2011.03.007
31. Aldahdooh M.A.A., Muhamad Bunnori N., Crack classification in reinforced concrete beams with varying thicknesses by mean of acoustic emission signal features, Construction and Building Materials 2013;45:282–288. https://doi.org/10.1016/j.conbuildmat.2013.03.090
32. Adamczak-Bugno A., Lipiec S., Adamczak J., Vičan J., Bahleda F., Identification of destruction processes and assessment of deformations in compressed concrete modified with polypropylene fibers exposed to fire temperatures using acoustic emission signal analysis, numerical analysis, and digital image correlation, Materials 2023;16:6786. https://doi.org/10.3390/ma16206786
33. Adamczak-Bugno A., Lipiec S., Koteš P., Bahleda F., Adamczak J., Detection of destructive processes and assessment of deformations in pp-modified concrete in an air-dry state and exposed to fire temperatures using the acoustic emission method, numerical analysis and digital image correlation, Polymers 2024;16:1161. https://doi.org/10.3390/polym16081161
34. Pistol K., Weise F., Meng B., Schneider U., The mode of action of polypropylene fibres in high performance concrete at high temperatures, in: RILEM Publications SARL, 2011.
35. Abdullah A.I., Lateef A.M., Innovative method for reinforcing beams with different types of concrete using cross-rod steel bracing under pure torsion, Civil Engineering Journal 2024;10:1093–1112. https://doi.org/10.28991/CEJ-2024-010-04-06
36. Major Z., Bodnár L., Merczel D.B., Szép J., Lublóy É., Analysis of the heating of steel structures during fire load, Emerging Science Journal 2024;8:1–16. https://doi.org/10.28991/ESJ-2024-08-01-01
37. Djamaluddin R., Irmawaty R., Fakhruddin, Yamaguchi K., Flexural behavior of repaired reinforced concrete beams due to corrosion of steel reinforcement using grouting and FRP sheet strengthening, Civil Engineering Journal 2024;10:222–233. https://doi.org/10.28991/CEJ-2024-010-01-014
38. Fares H., Noumowe A., Remond S., Self-consolidating concrete subjected to high temperature: Mechanical and physicochemical properties, Cement and Concrete Research 2009;39:1230–1238. https://doi.org/10.1016/j.cemconres.2009.08.001
39. Phan L., Fire performance of high-strength concrete: A report of the state-of-the art, Maryland, 1996.
40. Aldahdooh M.A.A., Bunnori N.M., Megat Johari M.A., Damage evaluation of reinforced concrete beams with varying thickness using the acoustic emission technique, Construction and Building Materials 2013;44:812–821. https://doi.org/10.1016/j.conbuildmat.2012.11.099
41. Colombo I.S., Main I.G., Forde M.C., Assessing damage of reinforced concrete beam using "b -value" analysis of acoustic emission signals, Journal of Materials in Civil Engineering 2003;15:280–286. https://doi.org/10.1061/(ASCE)0899-1561(2003)15:3(280)
42. Neimitz A., Lipiec S., Fracture toughness correction due to the in- and out-of-plane constraints, Theoretical and Applied Fracture Mechanics 2021;112:102844. https://doi.org/10.1016/j.tafmec.2020.102844
43. Residual Mechanical Properties and Durability of High-Strength Concrete with Polypropylene Fibers in High Temperatures, (n.d.). https://www.mdpi.com/1996-1944/15/13/4711 (accessed October 22, 2025).